Sensing Based Semi-deterministic Inter-Cell Interference Map in Heterogeneous Networks

Fatima Zohra Kaddour, Dimitri Kténas(✉), and Benoît Denis

Cea-Leti, Minatec Campus, 17 Rue des Martyrs, 38054 Grenoble, France
dimitri.ktenas@cea.fr

Abstract. This paper describes a low computational complexity semi-deterministic Inter-Cell Interference (ICI) map construction procedure. The built Interference Map (IM) gives the ICI level at each pixel of a two-dimensional area, based on an initialization map and ICI levels measured by collaborative User Equipments (UEs). In a first step, the initialization map is obtained with an analytical location-dependent ICI prediction model based on the Poisson Point Process (PPP) framework, where a priori deterministic information about the indoor/outdoor UE status can be injected. The analytical interference map is then updated following a self-learning approach, after spatially interpolating the gap sensed by the UEs with respect to analytical predictions in their visited positions. Two conventional spatial interpolation techniques are thus considered under regular and irregular sensing grids: Inverse Distance Weighting (IDW) and kriging, where exponential and Von Kàrmàn variograms are used. In order to show the benefits of the IM initialization, the performance is compared to that of traditional approaches (i.e., direct spatial interpolation of the ICI measured values), while varying the density of sensing positions.

Keywords: Inter-Cell Interference (ICI) · Interference Map (IM) · Self-learning · Spatial interpolation · Kriging · Long Term Evolution

1 Introduction

The emerging wireless communication standard Long Term Evolution Advanced (LTE-A) and beyond introduces significant technological enhancements to meet the ambitious requirements set by the Third Generation Partnership Project (3GPP) in terms of high data rate and high spectral efficiency.

To satisfy this continuous growth, the network is brought closer to the users by making the cells smaller [1]. However, a cell densification generates a high Inter-Cell Interference (ICI) level that should be mitigated in order to preserve high performance and satisfy the User Equipment (UE) Quality of Service (QoS). ICI estimation has been identified as a priority research topic in the recent literature. Some studies assume that the ICI follows a Gaussian distribution (by invoking the central limit theorem) and derive the ICI statistical parameters accordingly, as given in [2]. However, higher layer algorithms (e.g., handover, resource

D. Noguet et al. (Eds.): CROWNCOM 2016, LNICST 172, pp. 179–191, 2016.
DOI: 10.1007/978-3-319-40352-6_15

scheduling, coordinated base stations' transmission activity...) usually require more accurate channel estimations/predictions. Accordingly, current researches focus on the construction of refined Interference Maps (IMs) that aim at representing the ICI level as a function of the UE location in 2D spaces. Such maps are even more welcome and beneficial in Heterogeneous Networks (HetNets), which consist of different layers (i.e., macro and micro cells).

IMs can be designed using: (i) fingerprinting techniques (deterministic approach), or (ii) (location-dependent) ICI prediction models (e.g., stochastic approach). The high resolution fingerprinting approach consists in collecting real ICI levels with a drive test to measure the Received Signal Strength (RSS) at each location of the considered area [3,4]. This method needs a pre-training step, which may be too greedy in terms of time, or alternatively, blind crowd-sourcing (i.e., performing calibration "on the fly" as UEs physically sense and report their ICI conditions). The latter method requires that a minimum amount of field measurements are collected to converge properly and ensure uniform coverage. Thus it may introduce significant latency in the system (e.g., before being able to take any reliable IM-based decision). To overcome this drawback, low resolution fingerprinting (where the ICI levels can also be collected from collaborating UEs that send their locations and RSS measurements to the eNB) is exploited by estimating the ICI level of the non-visited locations using well-known spatial interpolation techniques [5,6]. The performance thus depends mainly on the accuracy of the used spatial interpolation technique. However, it may also suffer from similar latency issues under too sparse sensing. Moreover, both high and low resolution fingerprinting approaches can just account for an instantaneous picture of the ICI conditions (most likely, corresponding to distant sensing epochs) but not for varying base stations activity over time. On the contrary, ICI prediction models derive an analytical expression for the average ICI level as a function of UEs locations based on a priori stochastic assumptions (typically, regarding the spatial distribution of fixed interfering base stations) [2,7]. They represent a flexible alternative to cope with HetNets complexity. This may come at the expense of a tolerated mapping accuracy degradation (e.g., local prediction biases), somehow resulting from spatial interference averaging or even from deliberate approximations made for the sake of tractability (e.g., about distance-dependent integration bounds) in a few particular proposals [8].

In this study, we introduce a new mixed semi-deterministic method to dynamically build the IM. First of all, interference values are predicted by a stochastic location-dependent ICI analytical model proposed in our previous work [8] in a 2D area. Then prediction errors, which account for the deviation between the previous IM predictions and the deterministic UE measurements at the visited positions (i.e., at the discret sensing positions), are spatially interpolated to get a global prediction error surface. The latter can be further used to correct and update the final IM in a self-learning way (See Fig. 1). In comparison with classical approaches, where the UE measurements are directly interpolated,

the proposed solution is expected to converge more rapidly[1] towards the actual ICI conditions under spatially sparse sensing conditions. In the two compared IM approaches, conventional techniques are considered for the respective spatial interpolation steps, namely the Inverse Distance Weighted (IDW) technique and the Kriging technique with both exponential and Von Kàrmàn variogram models [9,10].

Numerical results are provided for illustration, based on deterministic Ray-Tracing radio simulations in a representative urban scenario and for different rates of regularly and irregularly drawn active UEs.

Overall, the novelty of this study lies in (i) the practical description of the IM initialization out of the predictive model in [8], while introducing local partitioning of the 2D prediction space around physical sensing positions, (ii) the coupling of this IM initialization with additional deterministic Indoor/Outdoor information and finally, (iii) the dynamic IM update depending on sensing positions through the spatial interpolation of prediction errors.

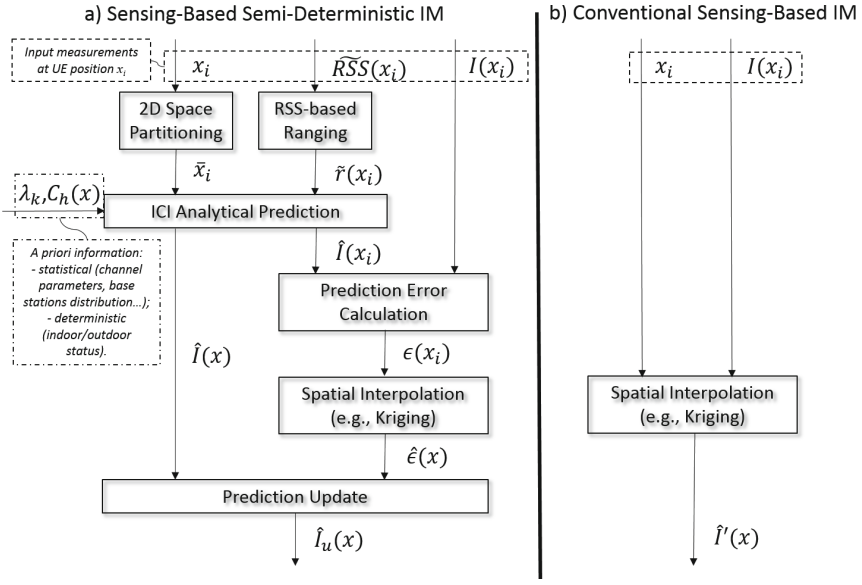

Fig. 1. Block diagrams of both proposed (a) and conventional (b) sensing-based IM approaches.

The paper is organized as follows. In Sect. 2 we define the system model. The semi-deterministic interference map construction steps are detailed in Sect. 3.

[1] The so-called "convergence speed" is just intended here in terms of the overall amount of collected UE measurements, indifferently of their acquisition conditions (i.e., synchronous measurements at distributed static UEs, asynchronous measurements under UE(s) mobility).

Section 4 summarizes the simulation parameters and the numerical results. Finally, Sect. 5 concludes the paper.

2 System Model

Our goal is to build a semi-deterministic interference map, where the IM is first initialized according to an analytical location-dependent ICI estimation model. Then a self-learning procedure allows an update of the IM according to the prediction errors obtained regarding the ICI levels sensed by the UEs in the visited positions. The analytical location-dependent ICI estimation model is based on stochastic approach, where in K-tier HetNets, the network's nodes are modeled according to an independent Poisson Point Process (PPPs). Let K be the total number of tiers in the network. Thus, the nodes positions of each tier k are modeled with an independent homogeneous PPP $\varphi_k = \{y_1, y_2, \dots\},\ k = 1, \dots, K$ of intensity λ_k.

The Orthogonal Frequency Division Multiple Access (OFDMA) technique is considered for resource allocation. Thereby, the intra-cell interference is canceled and the total interference received by a user u on the downlink is caused only by the nodes transmitting on the same frequency band. However the macro and small cell base stations can be allowed to transmit in the same frequency band (i.e., co-channel deployment), or in separate frequency band. When the macro and small cell BSs operate in different frequency bands, the ICI is called a co-tier interference, which means that the interference is generated between network elements on/belonging to the same layer. The macro cell users and the small cell users are interfered only by the macro cell base stations and the small cell base stations, respectively. Unlike the separate frequency band allocation, in a co-channel deployment, the users are interfered by all the network nodes without distinction between tiers. In this case, the interference is called a cross-tier interference.

In [8], both co-tier and cross-tier location-dependent ICI estimation model are derived. However, in this paper, we focus only on the co-tier interference. Without loss of generality, the same methodology can be used to apply the semi-deterministic approach in a cross-tier interference map construction.

The analytical model considers various sources of channel variations. A standard path loss function that depends on the distance $r_j = \|y_j\|$ between the user[2] and the interfering base station j is used. First (of all) the path loss function is classically expressed by $Pl(r_j) = l\ r_j^{-\gamma}$, where l and $\gamma > 2$ are respectively the reference (constant) path loss and the path loss exponent. Their values depend on the considered scenario (i.e., macro or small cell scenario), and can be instantiated by using the corresponding model specified in [11,12]. In addition, Rayleigh fast fading effects of the form $h \sim \exp(1)$ are taken into account. In [13], it has been shown that shadowing has a considerable impact on the ICI level. Thus, in our study a log-normal shadowing $\chi = 10^{\frac{X}{10}}$ such that $X \sim \mathcal{N}(\mu, \sigma)$ is

[2] For straightforward mathematical analysis, the user is assumed to be located at the origin.

considered while deriving the ICI estimation model. μ and σ are, respectively, the shadowing mean and standard deviation in dB. We depict as μ_k and σ_k the specific shadowing parameters associated with the k^{th} tier. Based on these radio environment parameters, a location-dependent analytical model of the downlink ICI level is given by:

$$\hat{I}(x) = \left(\frac{\pi \lambda_k^{(e)} \Phi(r, R_{ob}, 4)}{2\sqrt{\eta}\mathrm{erfc}^{-1}(0.5)} \right)^2 \quad (1)$$

where $\Phi(r, R_{ob}, 4) = \arctan(R_{ob}) - \arctan(r)$, r is the true distance between the UE and the first interfering eNB, $R_{ob} \simeq 3r$ is the radius of the observing area (i.e., the distance beyond which the interfering signal is considered negligible) and $\eta = \frac{1}{P_k \, l}$, where p_k is the node's transmission power of tier k. For more details regarding this model, please refer to [8].

Using the latter equation as a practical prediction tool in a real system (while assuming that eNB positions are unknown and/or non-disclosed to the UE), for any particular occupied position x_i of the 2D area of interest, $r(x_i)$ could be practically estimated as $\widetilde{r}(x_i)$ relying on the RSS perceived from the closest interfering eNB, $\widetilde{RSS}(x_i)$. Then the set of neighboring positions $\bar{x}_i$ around each occupied position x_i defines a region where one can assume in first approximation that $\widetilde{r}(x_i)$ is an acceptable common distance to the closest interfering eNB, $\forall x \in \bar{x}_i$. For instance, those regions, which do not necessarily coincide with eNB coverage cells, can be defined in a Voronoi sense around the sensing points (ensuring at least that any point in the region is closer to the sensing point leading to the common r approximation). Accordingly, the entire 2D area can be partitioned into small sub-areas of constant nominal ICI levels depending on the physically visited positions, as illustrated within the simplified 1D scenario of Fig. 2. Even under relatively low sensing points density, anyway much lower than the density simulated hereafter while evaluating the proposed solution, the assumption of a "common closest interfering eNB per region" has been reasonably validated by additional simulations (not shown here due to the limited number of pages). Extra deterministic a priori information, $C_h(x) = \{Indoor, Outdoor\}$, regarding the environment status at any position x can be used to account for lower perceived ICI levels in indoor zones, by adding an extra power penalty on top of the initial analytical prediction, while assuming Non Line of Sight (NLoS) outdoor channel parameters by default. Overall, the combination of analytical predictions, space partitioning and deterministic information leads to a piece-wise IM initialization $\widehat{I}(x)$, $\forall x$ in the 2D area of interest.

3 Inter-Cell Interference Map Construction and Updates

So as to get more reliable information, the previous IM initialization is updated following a self-learning procedure. For this sake, one can perform either a statistical shape analysis such as the Procrustes analysis, which defines the required transformations to be applied to the initial map based on the observed shape

deviations (i.e., scaling, rotation...) [15], or more simple interpolation techniques. As defined in the 3GPP standard, the active UEs report their measurements to the eNB. Accordingly, the observed "gap" between the measured ICI level and the estimated level can be evaluated at all the visited sensing points x_i, as illustrated in Fig. 2. Since the active UEs can be sparsely (i.e., under low deployment density) and/or non-uniformly distributed in the geographic area of interest, the IM is thus herein updated by spatially interpolating the perceived prediction errors as follows:

$$\epsilon(x_i) = \hat{I}(x_i) - I(x_i) \tag{2}$$

where, $\hat{I}(x_i)$ and $I(x_i)$ are respectively the estimated and the observed ICI levels at the sensing position x_i.

Finally, the corrected ICI value $\hat{I}_u(x)$ is defined by:

$$\hat{I}_u(x) = \hat{I}(x) - \hat{\epsilon}(x) \tag{3}$$

where, $\hat{I}(x)$ and $\hat{\epsilon}(x)$ are respectively the theoretical ICI level obtained by the stochastic location-dependent ICI model over partitioned regions and the interpolated gap at any position (i.e., including non-visited points).

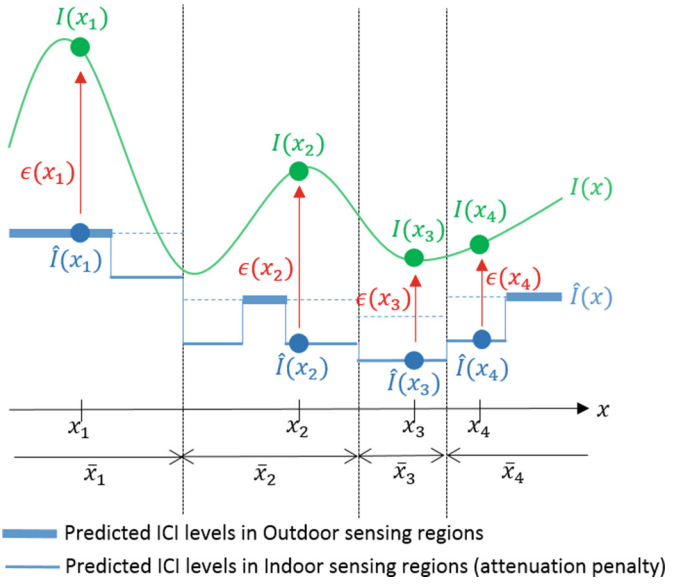

Fig. 2. Analytical ICI prediction errors based on visited UE sensing positions.

So as to estimate the gap $\hat{\epsilon}(x)$ at any location x, we consider classical spatial interpolation techniques that are widely used in the context of radio environment cartography [5,16,17]. More specifically, we focus on the well-known IDW and Kriging methods. These two approaches rely on a set of neighborhood observed gap values, through weighted linear combinations.

For IDW, the ICI gap values at unobserved positions are expressed as:

$$\hat{\epsilon}(x) = \sum_{i=1}^{N} \lambda(x_i)\epsilon(x_i) \tag{4}$$

where

$$\lambda(x_i) = \frac{d(x, x_i)^p}{\sum_{i=1}^{N} d(x, x_i)^{-p}} \tag{5}$$

is the Shepard's weighting function, given according to the distance between the location of the unobserved gap value x and the location of the observed gap values x_i, N is the number of considered observed gap values, and p is a real positive power (usually p is set to 4 or 6).

Unlike the IDW technique, the Kriging weights are based on the spatial correlation between the considered observations, which can be reflected by the covariance matrix C such that,

$$C(\tau)\lambda = C(0) \tag{6}$$

where $C(\tau)$ is the covariance matrix between the sensing positions x_i, $\tau = d(x_i, x_j)$ with $1 \leq i \leq N$ and $1 \leq j \leq N$. and $C(0)$ is the covariance vector between the interpolation position x and the sensing positions x_i.

An alternative way to describe the spatial relationship of the observed values is the variogram (or semi-variogram). Contrarily to the covariance matrix, the variogram can be calculated even if the mean of the observation values is unknown. Thus, the variogram is more convenient to describe the spatial relationship inside a data set and is described as,

$$\gamma(\tau) = \frac{1}{2} Var[\epsilon(x_i) - \epsilon(x_i + \tau)] \tag{7}$$

Under the hypothesis of first and second order stationarity, the semi-variogram is given as:

$$\gamma(\tau) = C(0) - C(\tau) \tag{8}$$

The experimental semi-variogram is calculated from the given data and therefore a discrete and often irregularly sampled function. The experimental variogram can then be approximated through a continuous parameter model. The most frequently used in the radio environment cartography are:

– the exponential model defined as:

$$\gamma(\tau) = n + c(1 + \exp(\frac{-3\tau}{r_g})) \tag{9}$$

With, n is the nugget, c is the sill and r_g is the range of the variogram (i.e. the correlation length).

– the Von Kàrmàn model defined as:

$$\gamma(\tau) = \frac{c}{2^{\nu-1}\Gamma(\nu)}(\frac{\tau}{r_g})^{\nu} K_{\nu}(\frac{\tau}{r_g}) \tag{10}$$

where Γ is the gamma function, K_{ν} is the modified Bessel function of the second kind of order $0 \leq \nu \leq 1$ [18].

4 Simulation Parameters and Performance Analysis

In the following simulations, the active UEs' ICI measurements (i.e., at visited positions x_i), as well as the true generalized ICI level $I(x) \forall x$, are taken from a realistic interference map obtained by ray-tracing techniques [14] over a mixed Indoor/Outdoor urban area of 1 km^2. Both the IDW and the Kriging (using exponential and Von Kàrmàn variogram models) interpolation techniques are first compared. We consider that the sensing task (i.e., ICI measurements) is performed by active UEs. Thus, the number of sensing positions is proportional to the population density and the rate of active UEs in the area. Regular and irregular sensing positions are considered. We assume that the studied area is in the city of Paris (France) with a population density of 21564 pop. per km^2 [19], which are equipped with mobile phones that can collaborate to the sensing procedure during their active mode, with an active UE rate of 45 %.

As a first step, comparing the so-called "true" IM over the whole area (i.e., obtained by ray-tracing deterministic simulations) with that obtained through low resolution fingerprinting (i.e., using a spatial interpolation over the deterministic ICI values at the sensing positions) based on the IDW and the Kriging methods, we obtain the Cumulative Distribution Functions (CDFs) of ICI level estimation error illustrated in Fig. 3. From the latter, we notice that the ICI error obtained with regular sensing positions is close to that of irregular sensing positions, whatever the interpolation technique. At the 50-percentile, IDW generates an ICI error of 6 dB, whereas kriging generates an error of about 2 dB independently of the used variogram model. The better performance of the kriging method is due to the weighting strategy, which relies on data correlation. It is worth noting that using the exponential variogram model generates lower ICI prediction errors. However the performance gap obtained with the two variogram models is very small (in the order of 0.01 dB). Based on this numerical results, in the following we focus only on the kriging method with the exponential variogram.

Next, in order to show the benefits from IM initialization, we compare the performance of the new proposed algorithm (i.e., IM update procedure) with the conventional low resolution fingerprinting technique that directly interpolates the sensed ICI values (see Fig. 1). We just assume perfect knowledge of the distance to the closest eNB at any point of the map for simplicity, considering the relatively high spatial density of sensing UEs (see the discussion on space partitioning validity in Sect. 2). The comparison is based on the CDF of ICI error with respect to the "true" IM (i.e., obtained by ray-tracing deterministic simulations) (see Fig. 4). As said before, the type of sensing grid has a relatively low impact on the performance under the considered practical UE density. The ICI obtained with the regular and the irregular sensing positioning is indeed very small. However, the performance of the updated IM is higher. At 90-percentile, the ICI error obtained with the updated IM (i.e., using the theoretical IM at the initialization step) is about 5 dB, whereas the latter is about 9 dB in case of low resolution fingerprinting. The a priori information provided by both the analytical IM and the indoor/outdoor map used in the initialization step allows

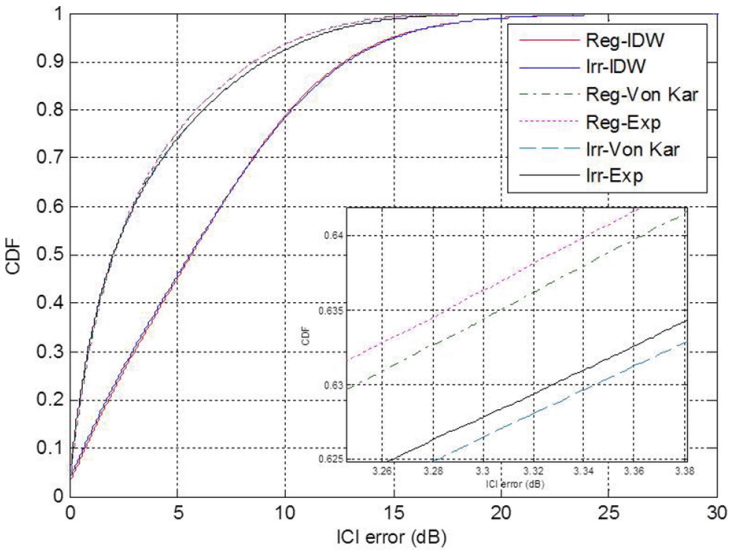

Fig. 3. CDF of ICI error in regular sensing positions

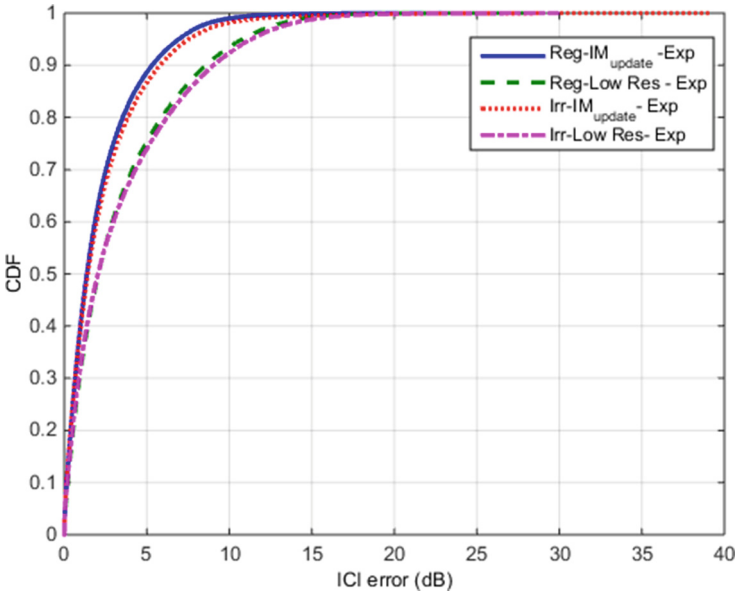

Fig. 4. CDF of ICI error: low resolution fingerprinting and updated IM

to smooth the observed gap values in comparison with the deterministic ICI values, while capturing even better local spatial correlation effects.

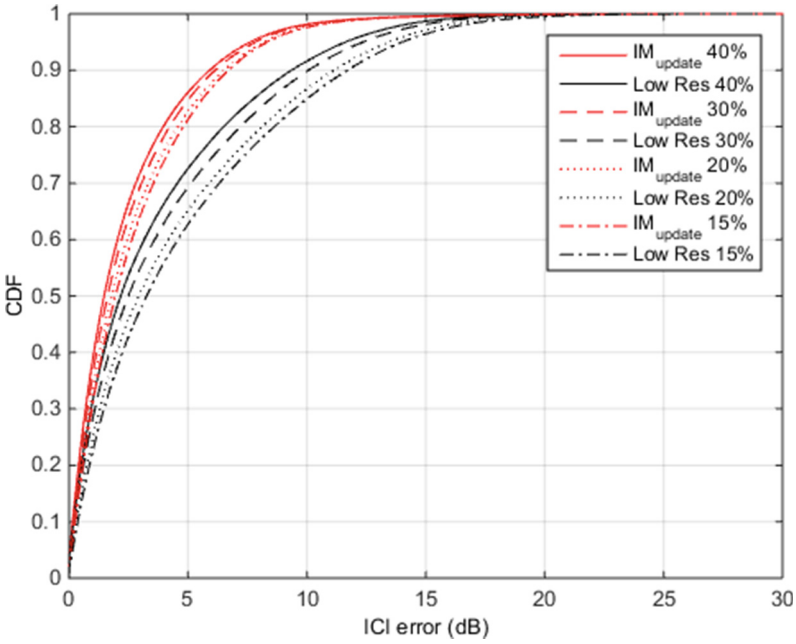

Fig. 5. CDF of ICI error: updated IM and Low resolution IM vs active UE rate (Colour figure online)

An active UE rate of 45 % may be high in practice and thus, not sufficiently realistic. Thus, the performance of the proposed updated IM is also studied with regards to different values in terms of active UEs rate. It is expected that under lower spatial density, the performances of both the updated IM and the low resolution fingerprinting techniques will decrease. We assume an irregular sensing positioning, where the updated IM and the low resolution fingerprinting IM are both generated with the kriging method based on the exponential variogram. Figure 5 shows the CDF of the corresponding ICI errors. The red and black curves represent the CDFs of ICI error obtained with the updated IM (i.e., the proposed algorithm) and the low resolution IM, respectively. The active UE rates are shown with different line types. We can notice that when the active UE rate decreases, the ICI error increases independently of the used technique for the IM construction. However, the updated IM generates a low ICI error compared to the low resolution fingerprinting technique. In addition, the gap introduced when the active UE rate decreases is higher in case of low resolution fingerprinting compared to the updated IM. At 90-percentile, when the active rate decreases from 40 % to 15 %, the ICI error of the updated IM increases from 5.92 dB to 6.63 dB, whereas the ICI error of the low resolution fingerprinting increases from 9.17 dB to 11.65 dB. In fact, even at low active UE rates (e.g., 15 %), the proposed algorithm outperforms the low resolution technique. This can be explained by the presence of an initialization step and by the update

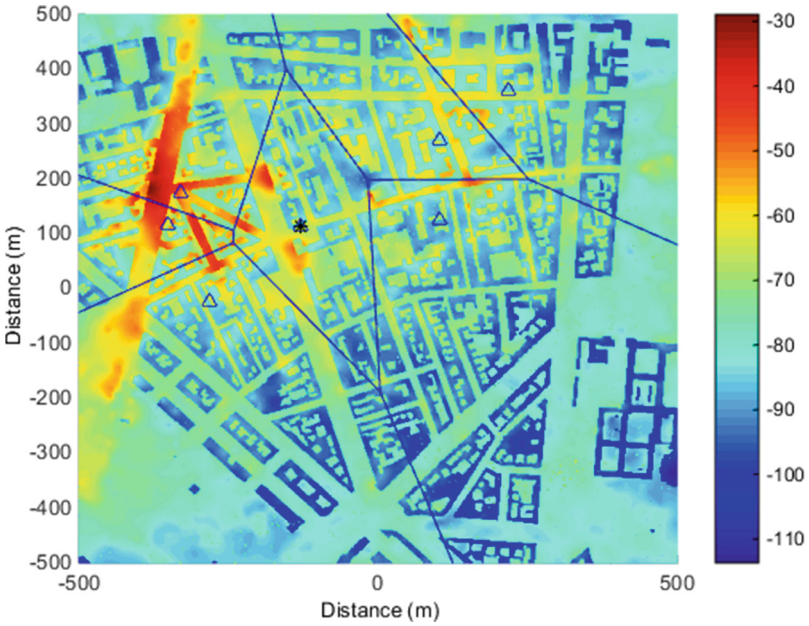

Fig. 6. Semi-deterministic IM based on exponential variogram: irregular sensing positions with active UE rate of 15 %

procedure according to the gap between the ICI level observed at the sensing positions and the theoretical IM at the same positions. It is also worth noting that this improvement is achieved with relatively low computational complexity. The additional computation cost inherent to our algorithm is related to the gap computation at the N sensing positions with a computational complexity of $\mathcal{O}(N)$. However, the complexity of (Eq. 4) can be decreased by considering only the closest neighboring sensing positions (i.e., choose the sensing positions within a radius $R \simeq 50$ m for the closest neighboring sensing positions). Figure 6 shows the resulting IM obtained with the proposed algorithm using the kriging interpolation with the exponential variogram, where an active UEs rate of 15 % is considered. The ICI levels are represented with a color code. Since the eNBs are located outdoor, the IM shows a low generated ICI level in indoor, a higher ICI level in outdoor, especially in the streets where UEs are exposed to more than one eNB in Line of Sight (LoS).

5 Conclusion

To build an IM, a stochastic-based location-dependent ICI estimation model that considers the shadowing, the fast fading and the path loss, was first developed. However, the analytical IM may be practically challenging to get reliable a priori information in real systems, due to the possibly low representativeness of the statistical model parameters in practical operating environments. Combining the

latter analytical IM with space partitioning and indoor/outdoor deterministic information enables piece-wise IM initialization when starting from scratch. To build a reliable IM, we propose an update of the analytical IM in a self-learning procedure. The update is performed by a spatial interpolation technique based on the ICI gap observed by collaborative UE at the sensing positions considered either regular and irregular. Two spatial interpolation techniques are studied: (i) Inverse Distance Weighting (IDW), and (ii) Kriging where exponential and Von Kàrmàn variogram model are investigated. The performance analysis shows that, unlike to the sensing positioning type, where the regular and irregular positioning sensing give a similar ICI estimation error, the choice of the spatial interpolation technique impacts more the ICI estimation performance. The numerical results show that the IDW is less reliable than the kriging spatial interpolation technique, since in the latter case the weights are based on the inputs correlations. The best ICI estimation is given with the kriging based on the exponential variogram. In addition, the performance of the proposed method is studied as a function of the active UE rate, where the performance of the updated IM degrades more slowly that for the low resolution fingerprinting method.

Acknowledgement. The research leading to this paper has been supported by the Celtic-Plus project SHARING (project number C2012/1-8).

References

1. Bhushan, N., et al.: Network densification: the dominant theme for wireless evolution into 5G. IEEE Commun. Mag. **52**(2), 82–89 (2014)
2. Pinto, P., et al.: A stochastic geometry approach to coexistence in heterogeneous wireless networks. IEEE JSAC **27**(7), 1268–1282 (2009)
3. Brunel, L., et al.: Inter-cell interference coordination and synchronization based on location information. In: Proceedings of WPNC 2010, April 2010
4. Rodrigues, M.L., et al.: Fingerprinting-based radio localization in indoor environments using multiple wireless technologies. In: Proceedings of IEEE PIMRC 2011, September 2011
5. Darakanath, R.C., et al.: Modeling of interference map for licensed shared access in LTE-advanced networks supporting carrier aggregation. In: Proceedings of IFIP Wireless Days 2013 (2013)
6. Kim, S.-J., et al.: Cooperative spectrum sensing for cognitive radios using Kriged Kalman filtering. IEEE J. Sel. Top. Sig. Process. **5**(1), 23–36 (2011)
7. Babaei, A., et al.: Interference statistics of a poisson field of interferers with random puncturing. In: Proceedings of IEEE MILCOM 2011, November 2011
8. Kaddour, F.Z., et al.: Downlink interference analytical predictions under shadowing within irregular multi-cell deployments. In: Proceedings of IEEE ICC 2015, June 2015
9. Shepard, D.: A two-dimensional interpolation function for irregularly-spaced data. In: Proceedings of ACM National Conference, pp. 517–524 (1968)
10. Krige, D.G.: A statistical approach to some mine valuations and allied problems at the Witwatersrand, Master's Thesis of the University of Witwatersrand (1951)

11. Evolved Universal Terrestrial Radio Access (E-UTRA); Further advancements for E-UTRA physical layer aspects (Release 9), 3Gpp. TR 36.814, v. 9.0.0 (2010)
12. Small Cell Enhancements for E-UTRA and E-UTRAN- Physical Layer Aspects (Release12), 3Gpp. TR 36.872, v. 12.1.0 (2013)
13. Kaddour, F.Z., et al.: A new method for inter-cell interference estimation in uplink SC-FDMA networks. In: Proceedings of IEEE VTC-Spring 2012, May 2012
14. Brau, M., et al.: Assessment of 3D network coverage performance from dense small-cell LTE. In: Proceedings of IEE ICC 2012, pp. 6820–6824, June 2012
15. Kendall, D.G.: Survey of the statistical theory of shape. Stat. Sci. **4**(2), 87–99 (1989)
16. Alaya-Feki, A., et al.: Informed spectrum usage in cognitive radio networks: interference cartography. In: Proceedings IEEE PIMRC 2008, September 2008
17. Seung-Jun, K., et al.: Cooperative spectrum sensing for cognitive radios using Kriged Kalman filtering. IEEE J. Sel. Top. Sig. Process. **5**(1), 24–36 (2011)
18. Sidler, R.: Kriging and Conditional Geostatistical Simulation Based on Scale-Invariant Covariance Models, Diploma Thesis, Institute of geophysics Department of Earth Science, October 2003
19. INSEE Recensement de 2012, Série historique des résultats du recensement de la population (2012)